

See discussions, stats, and author profiles for this publication at: <https://www.researchgate.net/publication/47348704>

Noncovalent Binding between Fullerenes and Protonated Porphyrins in the Gas Phase

ARTICLE *in* THE JOURNAL OF PHYSICAL CHEMISTRY A · OCTOBER 2010

Impact Factor: 2.69 · DOI: 10.1021/jp1033855 · Source: PubMed

CITATIONS

7

READS

38

3 AUTHORS, INCLUDING:



[Seung Koo Shin](#)

Pohang University of Science and Technol...

79 PUBLICATIONS 1,347 CITATIONS

[SEE PROFILE](#)

Noncovalent Binding between Fullerenes and Protonated Porphyrins in the Gas Phase

Sunghan Jung, Jongcheol Seo, and Seung Koo Shin*

Bio-Nanotechnology Center, Department of Chemistry, Pohang University of Science and Technology, San 31 Hyojadong Namgu, Pohang, Kyungbuk 790-784, Korea

Received: April 15, 2010; Revised Manuscript Received: August 23, 2010

Noncovalent interactions between protonated porphyrin and fullerenes (C_{60} and C_{70}) were studied with five different meso-substituted porphyrins in the gas phase. The protonated porphyrin–fullerene complexes were generated by electrospray ionization of the porphyrin–fullerene mixture in 3:1 dichloromethane/methanol containing formic acid. All singly protonated porphyrins formed the 1:1 complexes, whereas porphyrins doubly protonated on the porphine center yielded no complexes. The complex ion was mass-selected and then characterized by collision-induced dissociation with Xe. Collisional activation exclusively led to a loss of neutral fullerene, indicating noncovalent binding of fullerene to protonated porphyrin. In addition, the dissociation yield was measured as a function of collision energy, and the energy inducing 50% dissociation was determined as a measure of binding energy. Experimental results show that C_{70} binds to the protonated porphyrins more strongly than C_{60} , and electron-donating substituents at the meso positions increase the fullerene binding energy, whereas electron-withdrawing substituents decrease it. To gain insight into π – π interactions between protonated porphyrin and fullerene, we calculated the proton affinity and HOMO and LUMO energies of porphyrin using Hartree–Fock and configuration interaction singles theory and obtained the binding energy of the protonated porphyrin–fullerene complex using density functional theory. Theory suggests that the protonated porphyrin–fullerene complex is stabilized by π – π interactions where the protonated porphyrin accepts π -electrons from fullerene, and porphyrins carrying bulky substituents prefer the end-on binding of C_{70} due to the steric hindrance, whereas those carrying less-bulky substituents favor the side-on binding of C_{70} .

Introduction

Porphyrin–fullerene complexes held together by π – π interactions show the distance between flat porphyrin and curved fullerene somewhat to be shorter than the distance expected from stacked porphyrins.^{1,2} These complexes also provide novel photochemical properties that inspire the fabrication of diverse supramolecular assemblies for light-harvesting applications,^{3–5} in which porphyrins absorb light and donate active electrons to fullerenes.^{6–8} Although π – π interactions between planar molecules mostly result in parallel stacking structures,² those between flat and curved molecules afford diverse structures, from interleaved arrays^{9,10} to network structures,^{5,11,12} with a varying degree of electrostatic or charge transfer interactions.^{10,12} Metalloporphyrin dimers⁹ and free base porphyrins¹⁰ assemble into arrays with C_{60} in a zigzag motif, whereas porphyrins linked by palladium,⁵ lead,¹¹ or hydrogen bonds¹² construct the network structures with C_{60} . Composite nanoclusters of porphyrins and fullerenes are assembled around gold nanoparticles on tin oxide electrodes for the photocurrent generation.¹³

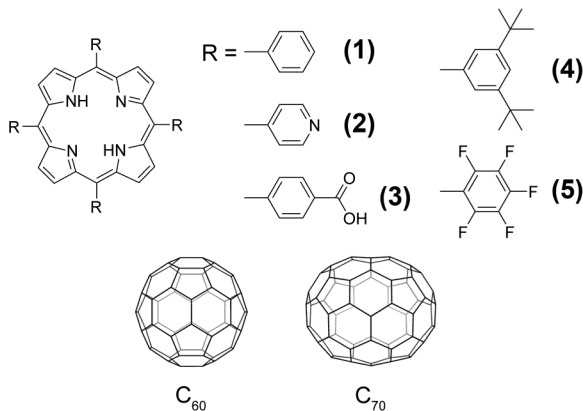
Interaction modes in various structures of porphyrin–fullerene complexes have been the subject of extensive studies in solution,^{4,14,15} in solid state,^{9,10} and on the solid surface.¹⁶ The binding constants of acyclic^{4,15} and cyclic¹⁴ porphyrin dimers with C_{60} and C_{70} were measured in solution. The complex structure and the porphyrin–fullerene distance were determined from crystallographic data.^{9,10} Self-assembly of porphyrin–fullerene supramolecular complexes was detected on the Ag(100) surface.¹⁶ The binding modes of porphyrin–fullerene complexes

were examined by high-level theory.^{17,18} In the gas phase, however, no binding studies of these complexes have been reported to date. Only the mass spectra of porphyrin–fullerene complexes were reported.^{15,19,20} For instance, the mass spectra of palladium-linked bisporphyrin–fullerene complexes were obtained using matrix-assisted laser desorption ionization mass spectrometry (MS),¹⁵ and those of cyclic metalloporphyrin dimer–fullerene complexes were obtained using electrospray ionization (ESI) MS.^{19,20} In addition, most of the condensed phase studies have provided information about ensemble-averaged interactions in complexes of various stoichiometries in the presence of solvent and counterion effects.^{4,9} To be more specific about intrinsic porphyrin–fullerene interactions, we need to employ a molecular probe that enables the measurement of the binding energy in the 1:1 complex. ESI offers a reproducible means to ionize nonvolatile molecules in solution into the gas phase,²¹ whereas tandem mass spectrometry (MS/MS) allows the energy-dependent studies of collision-induced dissociation (CID) of the mass-selected ion in the absence of solvent and counterions.^{22–24}

In the present paper, we employed ESI-MS/MS to study CID of protonated porphyrin–fullerene complex ions. We prepared the 1:1 complexes of protonated porphyrins with fullerenes (both C_{60} and C_{70}) by ESI and performed CID as a function of collision energy under single collision conditions with Xe. The relative collision energy inducing 50% dissociation ($E_{50\%}$) was determined from the CID yield-energy curve as a measure of the relative stability of the complex.

We employed five different meso-substituted porphyrins, as shown in Scheme 1: tetraphenyl porphyrin (**1**), tetra(4-pyridyl) porphyrin (**2**), tetra(4-carboxyphenyl) porphyrin (**3**), tetra(3,5-

* To whom correspondence should be addressed. E-mail: skshin@postech.ac.kr.

SCHEME 1: Meso-Substituted Porphyrins and Fullerenes Used in This Study

di-*tert*-butylphenyl) porphyrin (**4**), and tetra(pentafluorophenyl) porphyrin (**5**). All porphyrins have two nitrogens in the central porphine as the primary sites for protonation. In the case of porphyrin **2**, four pyridyl nitrogens are the additional protonation sites. Various meso-substituted porphyrins were chosen to examine the electronic effects of substituents on π – π interactions. Both spherical C₆₀ and ovoid C₇₀ were tested to differentiate the binding modes between “side-on” and “end-on” in protonated porphyrin–C₇₀ complexes. Protonated porphyrins were generated by adding formic acid into the ESI solvent (3:1 dichloromethane/methanol, v/v) and their charge states were determined by the number of protons attached to neutral porphyrin. To gain further insight into the π – π interactions, we calculated the proton affinity (PA), the highest occupied molecular orbital (HOMO) and the lowest unoccupied molecular orbital (LUMO) energies of porphyrin, and the binding energy of the protonated porphyrin–fullerene complex.

Experimental Section

Chemicals. Porphyrins **1** (97%), **2** (97%), **3** (75%), and **5** as well as fullerene (a mixture of C₆₀ and C₇₀) were purchased from Sigma-Aldrich (St. Louis, MO). Porphyrin **4** was generously given by Dr. P. D. W. Boyd, University of Auckland, New Zealand. HPLC-grade methanol and dichloromethane were purchased from J. T. Baker (Phillipsburg, NJ). All other chemicals were purchased from Sigma-Aldrich and used without further purification.

ESI Sample Preparation. A number of solvent systems were tested for ESI, including neat dichloromethane, toluene, 1,1,2,2-tetrachloroethane, and dimethylformamide as well as the 3:1 (v/v) mixture of each solvent with methanol. Of them, the 3:1 dichloromethane/methanol (v/v) mixture yielded the long-lasting signals for ESI-MS/MS experiments. Each ESI sample solution was prepared by dissolving either porphyrin (100 μ M) or fullerene (300 μ M) in the ESI solvent by sonication for 10 min. Porphyrin and fullerene solutions were mixed in a 1:1 ratio with 10 min sonication, and formic acid (0.5%) was added to the ESI sample solution.

Mass Analysis and Collision-Induced Dissociation. Experiments were carried out using a hybrid triple quadrupole/reflectron time-of-flight (TOF) mass spectrometer (QSTAR Pulsar-i, MDS Sciex, Concord, Canada) equipped with a nanospray ionization source, as previously described in detail.²⁵ A 1- μ m-i.d. Au/Pd-coated borosilicate glass tip (Proxeon, Odense, Denmark) was used to spray the sample into the mass spectrometer. The electrospray voltage was 1 kV, and both the

orifice and skimmer voltages were adjusted to the maximum ion intensity. The survey mass spectra were taken by transmitting ions through the three quadrupoles: Q0, Q1, and Q2. For MS/MS analysis, the precursor ion was mass-selected at Q1 and then accelerated into Q2 located inside a collision cell filled with Xe buffer gas. The product ions were analyzed by TOF in orthogonal geometry. The partial pressure of Xe was kept below 6.8×10^{-5} Torr to establish a single collision condition, in which the mean free path of an ion was equal to the 20 cm path length of the collision cell. On average, no more than one hard-sphere collision occurred within the cell.

The kinetic energy of an ion in the laboratory frame, E_{lab} , is the sum of the initial kinetic energy acquired in the ion source region and the potential energy gained by the voltage difference between Q0 and Q2. The initial kinetic energy was 5.31 ± 0.02 and 10.62 ± 0.04 eV for 1+ and 2+ ions, respectively, independent of mass.²⁵ The collision energy in the center-of-mass frame, E_{CM} , is expressed in eq 1.

$$E_{\text{CM}} = \left(\frac{m_{\text{Xe}}}{m_{\text{ion}} + m_{\text{Xe}}} \right) E_{\text{lab}} \quad (1)$$

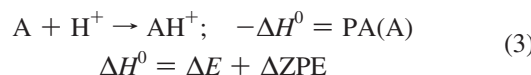
where m_{Xe} is the mass of Xe and m_{ion} is the mass of the precursor ion. The natural abundances of Xe isotopes are taken into account, as given in eq 2.

$$E_{\text{CM}} = \sum_j P_j \left(\frac{m_{\text{Xe}_j}}{m_{\text{ion}} + m_{\text{Xe}_j}} \right) E_{\text{lab}} \quad (2)$$

where P_j is the population of the j th isotope of Xe. The spread in natural isotopes of Xe contributes to 3.2% of an error in average collision energy. The spread in initial kinetic energy also contributes to the error in collision energy.

The CID product spectra of porphyrin–fullerene complexes were obtained as a function of collision energy, E_{CM} . The relative abundance of the precursor ion was fit to a Boltzmann sigmoid function to determine $E_{50\%}$ from the CID yield–energy curve. The uncertainty in curve fitting led to an error <3% in $E_{50\%}$ at the 95% confidence level.

Calculational Details. To evaluate PA and HOMO/LUMO energies, we optimized the geometries of neutral and protonated porphyrins at the Hartree–Fock (HF) level with a 3-21G basis set using Gaussian 03.²⁶ Harmonic vibrational frequencies were also calculated at the HF/3-21G level. Zero-point energy (ZPE) was obtained after scaling vibrational frequencies by a factor of 0.9085.²⁷ The HOMO energy was taken from the HF orbital energy, and the LUMO energy was calculated at the configuration interaction singles (CIS) level. The PA of porphyrin was determined from the negative of the enthalpy change at 0 K for reaction 3.²⁸



where ΔE is the total energy change and ΔZPE is the zero-point energy change. For porphyrin **4**, vibrational frequencies were not calculated because of limited computing resources. ΔZPE of porphyrin **4** was estimated from the average value of ΔZPE , because ΔZPE for the protonation of porphyrin was almost constant, independent of substituents.

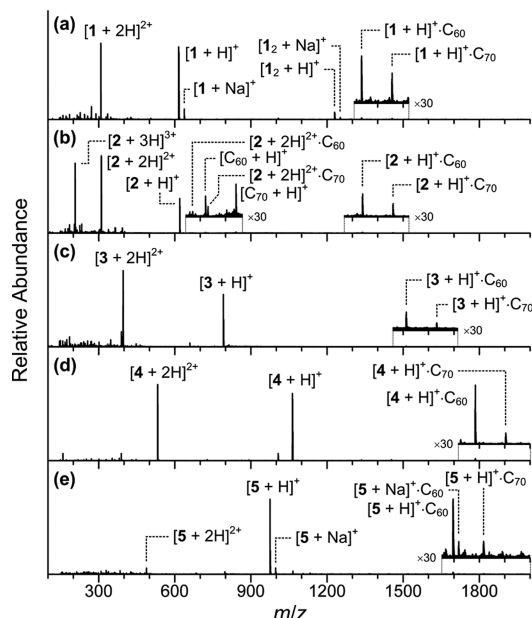


Figure 1. The ESI mass spectra of a 3:1 mixture of fullerene (C_m ; $m = 60, 70$) and porphyrin: (a) tetraphenyl porphyrin (**1**) + C_m ; (b) tetra(4-pyridyl) porphyrin (**2**) + C_m ; (c) tetra(4-carboxyphenyl) porphyrin (**3**) + C_m ; (d) tetra(3,5-di-*tert*-butylphenyl) porphyrin (**4**) + C_m ; (e) tetra(pentafluorophenyl) porphyrin (**5**) + C_m . Singly protonated porphyrins are denoted by $[n + H]^+$ ($n = \mathbf{1}-\mathbf{5}$), doubly protonated porphyrins by $[n + 2H]^{2+}$, triply protonated porphyrin **2** by $[2 + 3H]^{3+}$, sodiated porphyrins **1** dimer by $[1_2 + H]^+$ and $[1_2 + Na]^+$, and porphyrin–fullerene complexes by $[n + H]^+ \cdot C_m$, $[2 + 2H]^{2+} \cdot C_m$, and $[5 + Na]^+ \cdot C_m$. The porphyrin–fullerene spectral region is enlarged by 30 times.

For the binding energy calculation, the density functional theory (DFT) with the Perdew–Burke–Ernzerhof (PBE) functional was employed with a Slater-type double- ζ plus polarization (DZP) basis set using ADF 2009.01.^{29,30} Geometries of protonated porphyrin, fullerene, and protonated porphyrin–fullerene complex were optimized at the DFT/DZP level, and the binding energy of the protonated porphyrin–fullerene complex was calculated from the difference in energy between the porphyrin–fullerene complex (E_{complex}) and the porphyrin ($E_{\text{porphyrin}}$) plus fullerene ($E_{\text{fullerene}}$), as given in eq 4.

$$E_{\text{binding}} = E_{\text{porphyrin}} + E_{\text{fullerene}} - E_{\text{complex}} \quad (4)$$

Zero-point vibrational energy and basis-set superposition error (BSSE) were not corrected. The PBE functional without BSSE corrections was known to yield the $\pi-\pi$ interaction energies in good agreement with those in the literature.¹⁷

Results

ESI Mass Spectra of Porphyrins and Porphyrin–Fullerene Complexes. The ESI mass spectra of the porphyrin–fullerene mixtures are presented in Figure 1. All porphyrins yield both singly and doubly protonated ions, $[n + H]^+$ and $[n + 2H]^{2+}$ ($n = \mathbf{1}-\mathbf{5}$), indicating that the two central porphine nitrogens are the protonation sites. Porphyrin **2** results in the triply protonated ion, $[2 + 3H]^{3+}$, suggesting that the pyridyl nitrogens are also the protonation sites. Although the singly protonated porphyrins are seldom observed in solution,³¹ they are readily generated by ESI. The intensity ratio of $[n + 2H]^{2+}$ to $[n + H]^+$ is 1.05, 2.24, 1.46, 1.11, and 0.08 for porphyrins **1–5**, respectively. The relative abundance of $[5 + 2H]^{2+}$ is 13–27

times lower than those of $[n + 2H]^{2+}$ ($n = \mathbf{1}-\mathbf{4}$), indicating that the electron-withdrawing pentafluorophenyl substituents reduce the proton affinity. The intensity ratio of $[2 + 3H]^{3+}$ to $[2 + H]^+$ is 2.03, implying that the proton affinity of the pyridyl group is comparable to that of the central porphine. Of the five porphyrins, only porphyrin **1** results in the protonated dimer $[1_2 + H]^+$ with the relative abundance of 0.10, suggesting the formation of the π -stacked ion-induced dipole complex. In addition, both porphyrins **1** and **5** yield sodiated ions; $[1 + Na]^+$, $[1_2 + Na]^+$, and $[5 + Na]^+$.

Although fullerene alone provides no protonated species, neither $[C_{60} + H]^+$ nor $[C_{70} + H]^+$, the mixture of porphyrin **2** with fullerene surprisingly yields both $[C_{60} + H]^+$ and $[C_{70} + H]^+$ (Figure 1b). Because the other four porphyrins showing both singly and doubly protonated porphyrin ions exhibit no protonated fullerenes in the ESI mass spectra, we think that the triply protonated porphyrin $[2 + 3H]^{3+}$ is involved in the protonation of fullerenes. Nonetheless, this protonation process was not characterized further.

All of the singly protonated porphyrins result in the 1:1 porphyrin–fullerene complexes with relative abundances of 0.010–0.029 for $[n + H]^+ \cdot C_{60}$ and 0.005–0.011 for $[n + H]^+ \cdot C_{70}$. Of the doubly protonated porphyrins, only $[2 + 2H]^{2+}$ yields the 1:1 complex with the relative abundance of 0.005 and 0.01 for $[2 + 2H]^{2+} \cdot C_{60}$ and $[2 + 2H]^{2+} \cdot C_{70}$, respectively. Meanwhile, the triply protonated porphyrin $[2 + 3H]^{3+}$ yields no porphyrin–fullerene complex. Of the sodiated porphyrins, $[5 + Na]^+$ results in the complexes with fullerenes.

Collision-Induced Dissociation of Porphyrin–Fullerene Complexes. CID was performed on all of the 1:1 protonated porphyrin–fullerene complexes: $[n + H]^+ \cdot C_{60}$ ($n = \mathbf{1}-\mathbf{5}$), $[n + H]^+ \cdot C_{70}$ ($n = \mathbf{1}, \mathbf{2}, \mathbf{4}, \mathbf{5}$), $[2 + 2H]^{2+} \cdot C_{60}$, and $[2 + 2H]^{2+} \cdot C_{70}$, except for $[3 + H]^+ \cdot C_{70}$, in which the transmission efficiency was too low. The CID yield–energy curves are shown in Figure 2a–f, presenting the relative abundance of the precursor ion as a function of collision energy (E_{CM}). The representative MS/MS spectra obtained at the collision energy marked by an arrow are also displayed in insets of Figure 2. The singly protonated porphyrin–fullerene complex ion readily dissociates in the collision cell with the initial kinetic energy alone (5.31 ± 0.02 eV), although it is easily mass-selected in the second quadrupole (Q1).

On the other hand, $[2 + 2H]^{2+} \cdot C_m$ ($m = 60, 70$) remains stable, even at the initial kinetic energy of 10.62 ± 0.04 eV. In all cases, loss of neutral fullerene, either C_{60} or C_{70} , occurs exclusively. No protonated fullerenes result from collisional activation of the protonated porphyrin–fullerene complexes over the entire collision energy, suggesting that the protonated porphyrins neither transfer proton to fullerene nor form proton-bound complexes with fullerene. Thus, the protonated porphyrin–fullerene complexes are considered to be held together by noncovalent interactions consisting of the $\pi-\pi$ interaction between flat porphyrin and the curved fullerene and the charge-induced dipole interaction between the protonated porphyrin and the polarizable fullerene.

All of the CID curves are plotted together in Figure 2g to compare the descending slope around $E_{50\%}$, and the relative abundance of the product ion is presented on a semilog scale in Figure 2h to compare the product appearance near threshold. $E_{50\%}$ values are listed in Table 1. As the charge state increases from 1+ to 2+, the CID curves are shifted to higher energies, presumably due to an increase in charge-induced dipole interaction energy, which is proportional to the square of the charge. In the cases of the 1+ charge state complexes, $E_{50\%}$ for the loss

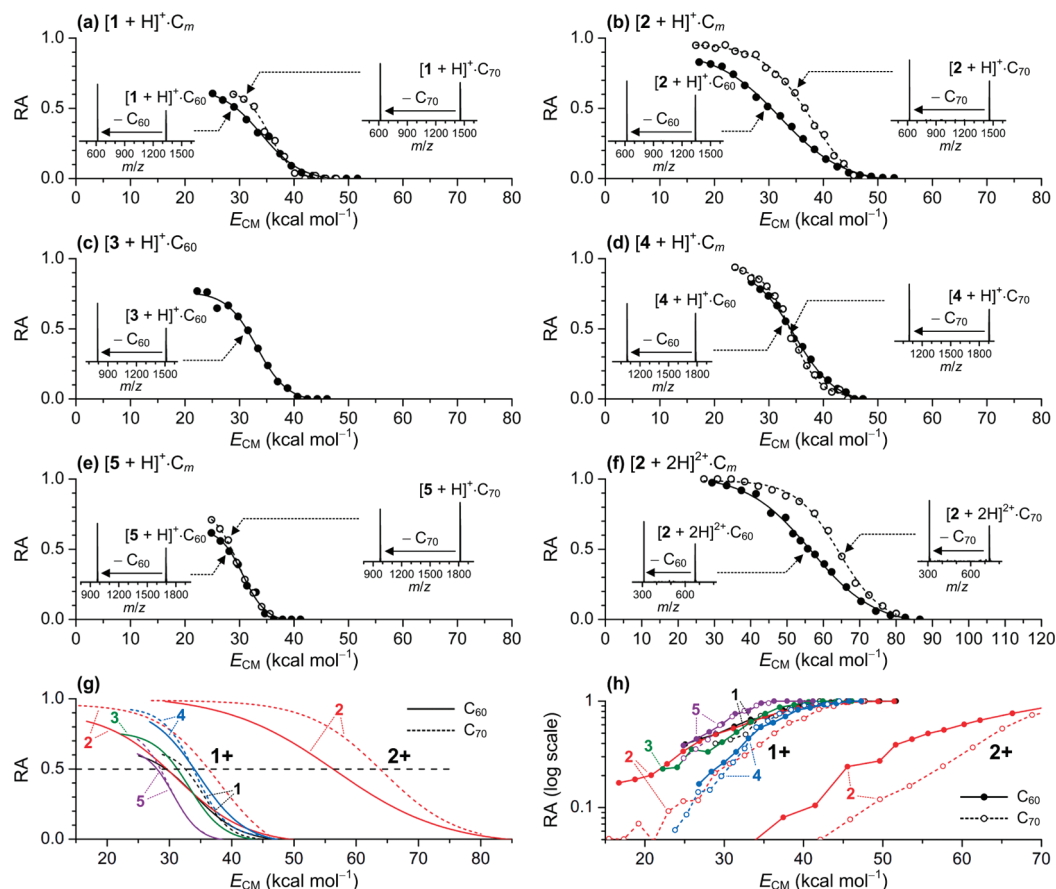


Figure 2. Relative abundance (RA) of the 1:1 protonated porphyrin–fullerene complex ion as a function of center-of-mass collision energy in kcal mol⁻¹: (a) $[1 + H]^+ \cdot C_m$, (b) $[2 + H]^+ \cdot C_m$, (c) $[3 + H]^+ \cdot C_{60}$, (d) $[4 + H]^+ \cdot C_m$, (e) $[5 + H]^+ \cdot C_m$, (f) $[2 + 2H]^{2+} \cdot C_m$ ($m = 60, 70$), (g) collision-induced dissociation (CID) curves for singly protonated (1+) and doubly protonated (2+) porphyrin–fullerene complexes, and (h) appearance of the product ion as a function of E_{CM} on a semilog scale. Insets in parts a–f show the CID mass spectra obtained at the collision energy marked by an arrow.

TABLE 1: $E_{50\%}$ and Binding Energy of the Protonated Porphyrin–Fullerene Complex (in kcal mol⁻¹)

protonated porphyrin	$E_{50\%}$ from experiment ^a		binding energy from theory ^b		
	C_{60}	C_{70}	C_{60}	C_{70} (end-on)	C_{70} (side-on)
$[1 + H]^+$	29 ± 1	32 ± 1	15.2	15.6	17.3
$[2 + H]^+$	30 ± 1	36 ± 1	16.2	16.6	18.5
$[3 + H]^+$	31 ± 1		14.8	15.6	17.4
$[4 + H]^+$	34 ± 1	34 ± 1	17.2	17.7	15.0
$[5 + H]^+$	28 ± 1	28 ± 1	15.2	15.5	16.1
$[2 + 2H]^{2+} (\text{py}^2)$	56 ± 2	64 ± 2	22.7	25.6	27.6

^a Errors are from the Xe isotope distribution and curve fitting.

^b Obtained at the DFT/DZP level.

of C_{60} lies in the 28–34 kcal mol⁻¹ range, whereas $E_{50\%}$ for the loss of C_{70} ranges from 28 to 36 kcal mol⁻¹. With the 2+ charge state of porphyrin **2**, the $E_{50\%}$ value increases to 56 and 64 kcal mol⁻¹ for the loss of C_{60} and C_{70} , respectively. The product appearance near threshold (Figure 2h) shows that C_{70} binds to the protonated porphyrin as strongly as C_{60} in all cases. The threshold energy for the loss of C_{70} is equal to or higher than that for the loss of C_{60} , regardless of the charge state or the type of meso substituents.

The energy range for the C_{60} -loss curve varies with the type of meso substituents (Figure 2g): Of the five different porphyrins, **5** having pentafluorophenyl groups displays the curve in the lowest energy region, and **4** containing 3,5-di-*tert*-butylphenyl groups shows the curve in the highest energy region, and **3**

carrying 4-carboxyphenyl groups presents the curve in the middle of **4** and **5**. The descending slope near $E_{50\%}$ is almost identical for porphyrins **3**–**5**. Meanwhile, **1** and **2** having unsubstituted phenyl and pyridyl groups, respectively, yield the C_{60} -loss curves lying between **4** and **5** with the slopes descending more slowly than porphyrins **3**–**5**. For both **4** and **5**, nearly identical C_{70} - and C_{60} -loss curves indicate that these two porphyrins having bulky meso substituents hardly distinguish C_{70} from C_{60} , favoring the “end-on” binding mode common to both ovoid C_{70} and spherical C_{60} . Meanwhile, the C_{70} -loss curves from both **1** and **2** are shifted to higher energies by 3 and 6 kcal mol⁻¹, respectively, as compared with the C_{60} -loss curves, suggesting that the two porphyrins having unsubstituted phenyl or pyridyl groups favor the “side-on” binding mode for ovoid C_{70} .

The fact that $E_{50\%}$ for the loss of C_{60} is almost identical to that of C_{70} in both **4** and **5** is interesting because the number of internal degrees of freedom (DOF) differs by 30 between C_{60} and C_{70} . In CID experiments, the short flight time (100–200 μ s for the 1+ ion, 75–120 μ s for the 2+ ion) of an ion in the collision cell leads to the kinetic shift in CID curve as the heat capacity of the ion increases with increasing size of DOF. In the cases of covalent compounds, in which the intramolecular vibrational redistribution is fast and statistical among all internal DOF, $E_{50\%}$ values need to be corrected for DOF.^{22,32,33} However, the DOF correction²² may not be necessary for the comparison of the binding of C_{60} with that of C_{70} to the same porphyrin, because porphyrin and fullerene are noncovalently bound with

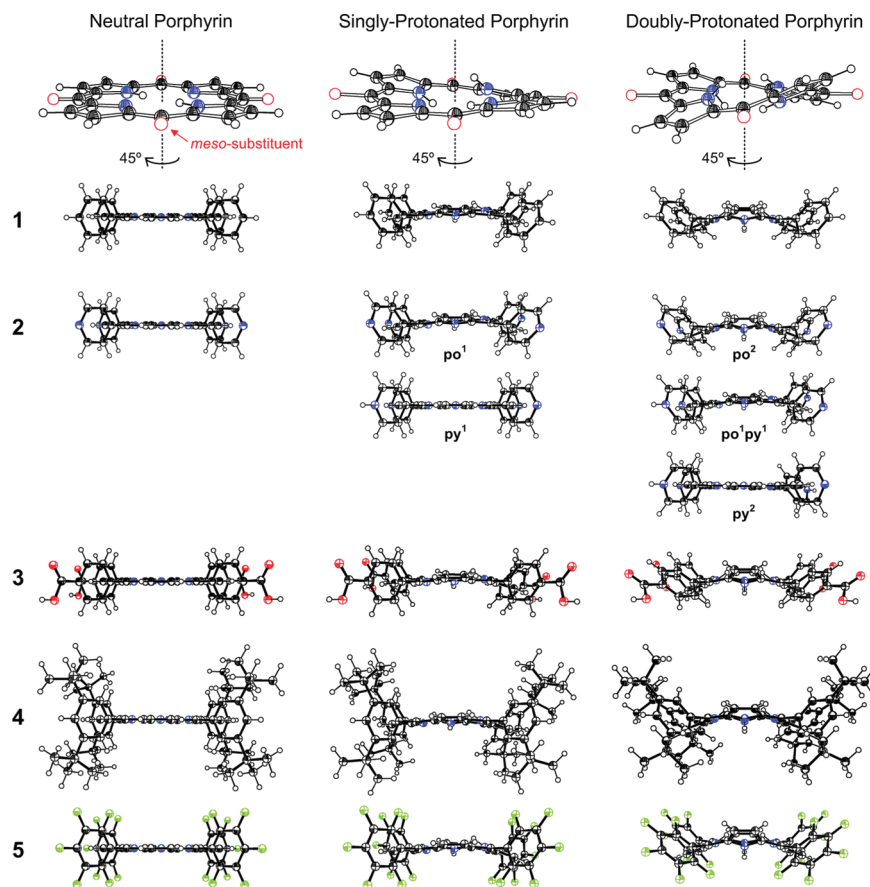


Figure 3. Structure of neutral (left), singly protonated (center) and doubly protonated (right) porphyrins **1–5**. Color code for atoms: blue, nitrogen; red, oxygen; black, carbon; green, fluorine. Small open circle denotes hydrogen, and large red circle represents the meso substituent. In porphyrin **2**, **po**¹ and **po**² refer to the single and double protonation on the porphine nitrogen, respectively, and **py**¹ and **py**² refer to the single and double protonation on the pyridyl nitrogen, respectively.

low-frequency, large-amplitude vibrational modes, and little intermolecular vibrational coupling is expected between the two moieties.

Structures of Neutral and Protonated Porphyrins. Structures of neutral and singly and doubly protonated porphyrins calculated at the HF/3-21G level are shown in Figure 3. The porphine plane is flat in a neutral system, puckered after single protonation, and twisted to a saddle shape after double protonation (see Figure 3, top). A similar saddle-shaped structure has been reported for unsubstituted phorphine diacid.³⁴ The single protonation on the porphine center makes the protonated pyrrolic ring with two adjoining methine bridges puckered out of plane by 20° in dihedral angle. The out-of-plane angle of proton on the imino nitrogen atom is ~20°. The double protonation on the porphine center causes the two NH protons in the opposite side to point upward and the other two NH protons to point downward in the saddle structure due to the repulsion among four NH protons. In neutral porphyrins (Figure 3, left), the phenyl or pyridyl substituents are aligned nearly perpendicular to the porphine plane, and the space above and below the porphine plane are equally available for fullerene binding. When the imino nitrogen of the pyrrolic ring is singly protonated (Figure 3, center), the two phenyl or pyridyl groups adjacent to the protonated pyrrolic ring rotate about 10–26° from the 90° dihedral angle, and the NH proton protrudes toward the center, thus hindering the fullerene's binding. When the two imino nitrogens of porphine are protonated (Figure 3, right), all of the four phenyl or pyridyl groups rotate about 17–33° from the 90° dihedral angle, and the two surfaces, one above and one below the twisted porphine plane, are equally hindered for

fullerene binding. In the case of **2** having 4-pyridyl meso substituents, there are two possible structures for singly protonated porphyrin (**po**¹ and **py**¹) and three structures for doubly protonated one (**po**², **po**¹**py**¹, and **py**²). The porphine plane remains flat (**py**¹ and **py**²) unless the pyrrolic nitrogen is protonated (**po**¹, **po**², and **po**¹**py**¹). When the pyridyl nitrogen is protonated, the protonated pyridyl group aligns perpendicular to the porphine plane after single protonation, but rotates about 15–30° from the 90° dihedral angle after double protonation.

Proton Affinity of Porphyrin and Electronic Effects of Meso Substituents on PA. Energy levels of the protonated porphyrins are compared in Figure 4. Those of the corresponding neutral species are set to zero. The calculated PA is also listed in Figure 4. Both the total and zero-point energies are summarized in Table S1 in the Supporting Information. The energy and enthalpy changes for the protonation reaction are listed in Table S2 in the Supporting Information.

The PA of fullerene (204 and 207 kcal mol⁻¹ for C₆₀ and C₇₀, respectively) is taken from the literature.³⁵ The first PA (PA₁) of porphine nitrogen is 29–59 kcal mol⁻¹ greater than PA of C₆₀ and increases in the order of **5** < **2** < **3** < **1** < **4**. The PA₁ of 250 kcal mol⁻¹ for unsubstituted porphine (**por**) is the same as PA₁ of porphyrin **3**. In the case of porphyrin **2**, the PA₁ of porphine nitrogen (246 kcal mol⁻¹) is 11 kcal mol⁻¹ greater than PA₁ of pyridyl nitrogen (235 kcal mol⁻¹). The second PA (PA₂) of porphine nitrogen is 67–72 kcal mol⁻¹ less than PA₁, but increases in the same order as PA₁ in the 163–196 kcal mol⁻¹ range, indicating strong repulsions between protons in the central porphine. The PA₂ of 168 kcal mol⁻¹ for **por** is much lower than the PA₂ of 181 kcal mol⁻¹ for porphyrin

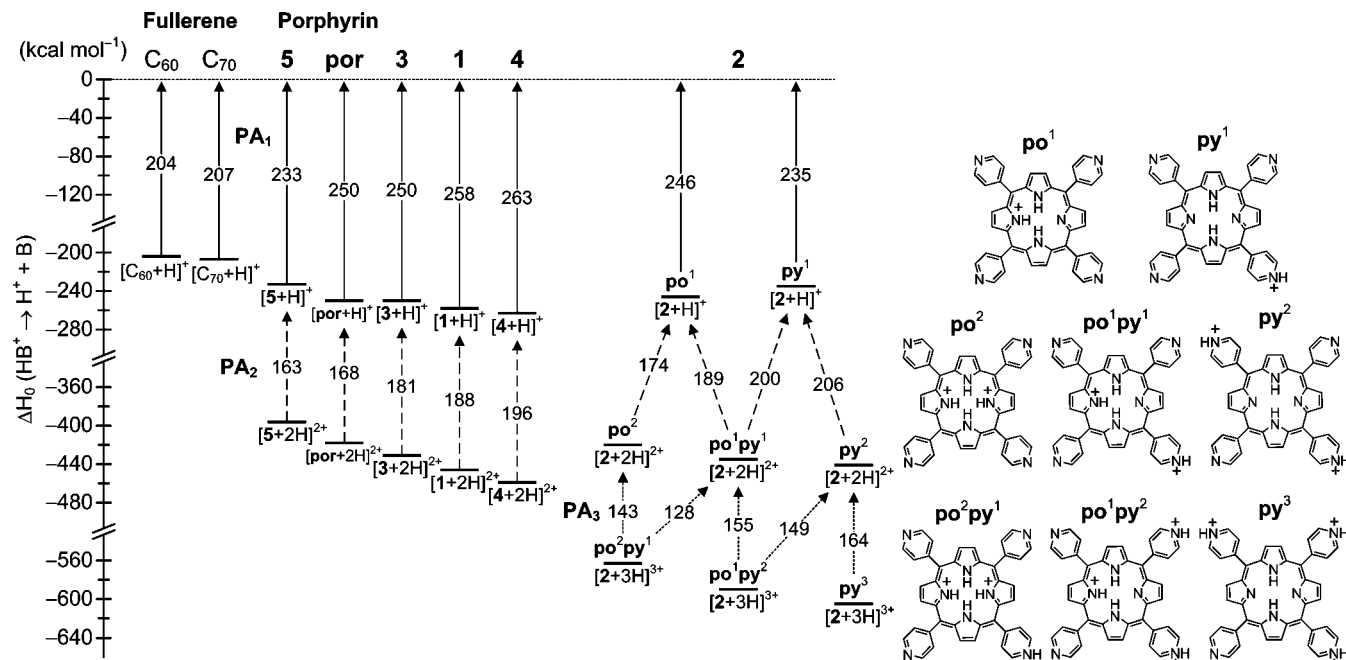


Figure 4. Proton affinity (PA) of porphyrins **1–5**, fullerenes (C_{60} and C_{70}), and unsubstituted porphine (**por**). The PA is listed in kcal mol^{-1} . PA_1 , PA_2 , and PA_3 denote the first, second, and third PA of a molecule calculated from the enthalpy change at 0 K. The protonation sites in different configurations of protonated porphyrin **2** are shown at right.

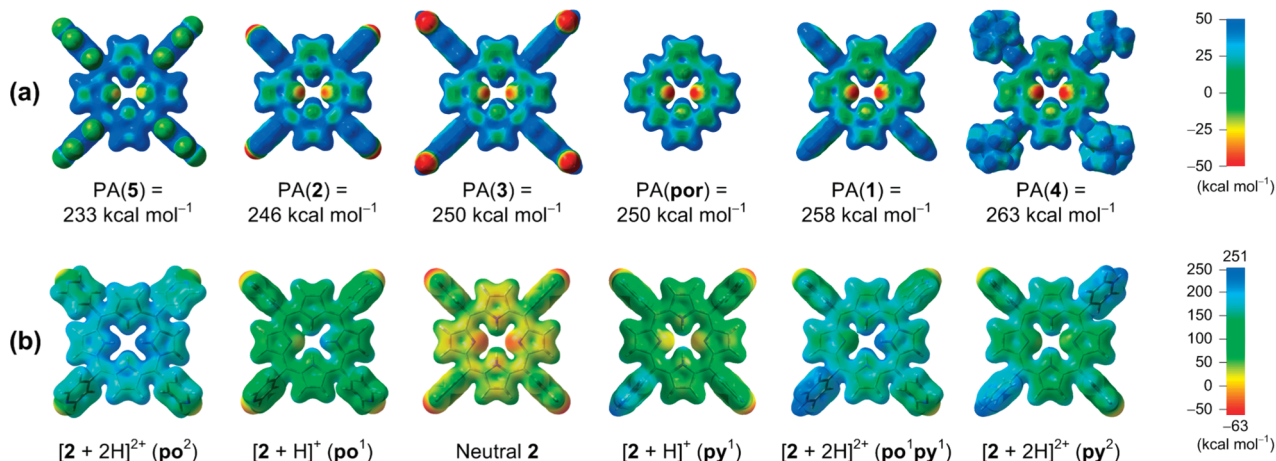


Figure 5. (a) Plots of ESP of neutral porphyrins **1–5** and **por** mapped onto electron density isosurfaces ($0.02 \text{ e}/\text{au}^3$) as well as the proton affinity (PA). The ESP at a given point is a measure of the electrostatic energy that a $1+$ test charge would experience at that point. The negative potential region (shown in red) is more electronegative than the positive potential region (shown in blue); (b) ESP plots of neutral and singly and doubly protonated porphyrin **2** as a function of the protonation site. ESPs are mapped onto electron density isosurfaces ($0.02 \text{ e}/\text{au}^3$). Although the ESPs of neutral porphyrin **2** are identical in the upper and lower panels, they look different because the scale bar changes from $100 \text{ kcal mol}^{-1}$ (-50 to 50) in the upper panel to $314 \text{ kcal mol}^{-1}$ (-63 to 251) in the lower panel.

3. For porphyrin **2**, the PA_2 of the porphine nitrogen ($174 \text{ kcal mol}^{-1}$) is 32 kcal mol^{-1} less than the PA_2 of pyridyl nitrogen ($206 \text{ kcal mol}^{-1}$). The third PA (PA_3) of pyridyl nitrogen is $164 \text{ kcal mol}^{-1}$.

Although the present computational level does not yield an absolute PA within chemical accuracy, PA values obtained here are useful in quantifying the electronic effects of meso substituents on the basicity of porphine nitrogen. The electronic effect is visualized by plotting electrostatic potentials (ESPs)³⁷ of neutral porphyrins in Figure 5a along with the PA. The ESP at a given point is a measure of the electrostatic energy that a $1+$ test charge experiences at that point.³⁶ The ESP at the porphine nitrogen becomes increasingly more negative in the order of **5** < **2** < **3** < **1** < **4**, in line with the increasing order of the PA of porphine. Porphyrin **3** shows an ESP on the porphine nitrogen almost identical to that of **por**, suggesting that the 4-carboxy-

phenyl group is electronically neutral, similarly to hydrogen. Thus, the pentafluorophenyl group in **5** is the most electron-withdrawing substituent, the pyridyl group in **2** is the weakly electron-withdrawing substituent, the phenyl group in **1** is the weakly electron-donating substituent, and the 3,5-di-*tert*-butylphenyl group in **4** is the most electron-donating substituent.

In the case of porphyrin **2**, both the proton affinity and relative stability depend on the site of protonation, as shown in Figure 4. In singly protonated porphyrin **2**, the po^1 configuration having a proton on porphine ($\text{PA}_1 = 246 \text{ kcal mol}^{-1}$) is more stable than the py^1 configuration having a proton on the pyridyl group (PA_1 of $235 \text{ kcal mol}^{-1}$). In doubly protonated porphyrin **2**, the py^2 configuration having two protons on the pyridyl groups in the opposite side (PA_2 of $206 \text{ kcal mol}^{-1}$) is the most stable, whereas the po^2 configuration having two protons on porphine is the least stable (PA_2 of $174 \text{ kcal mol}^{-1}$). In triply protonated

TABLE 2: Energies of the HOMO and the LUMO (in eV)^a and the HOMO–LUMO Energy Gap ($\Delta\epsilon$)

	neutral (P)			[P + H] ⁺			[P + 2H] ²⁺			[P + 3H] ³⁺		
	HOMO	LUMO	$\Delta\epsilon$	HOMO	LUMO	$\Delta\epsilon$	HOMO	LUMO	$\Delta\epsilon$	HOMO	LUMO	$\Delta\epsilon$
1	-6.54	-3.53	3.01	-9.78	-7.02	2.76	-12.73	-10.13	2.60			
2	-7.05	-4.04	3.01	-10.34 (po ¹)	-7.58	2.76	-13.66 (po ²)	-11.00	2.66	-15.73 (po ² py ¹)	-13.06	2.67
				-9.21 (py ¹)	-6.25	2.96	-12.49 (po ¹ py ¹)	-9.70	2.79	-14.53 (po ¹ py ²)	-11.74	2.79
3	-6.91	-3.90	3.01	-10.10	-7.35	2.75	-13.33	-10.70	2.63			
4	-6.39	-3.39	3.00	-9.47	-6.72	2.75	-12.19	-9.60	2.59			
5	-7.65	-4.62	3.03	-10.91	-8.18	2.73	-14.23	-11.52	2.71			
por	-6.64	-3.62	3.02	-10.26	-7.47	2.79	-13.99	-11.28	2.71			
C ₆₀	-7.6 ^b	-5.9 ^c	1.7 ^d									
C ₇₀	-7.47 ^e	-5.87 ^c	1.6 ^d									

^a Unless noted otherwise, HOMO and LUMO energies are from HF and CIS calculations, respectively. ^b Taken from ref 37. ^c Calculated from the HOMO–LUMO energy gap. ^d Taken from ref 39. ^e Taken from ref 38.

porphyrin **2**, the **py**³ configuration having three protons on pyridyl groups is the most stable, whereas the **po**²**py**¹ configuration having two protons on porphine and one proton on pyridyl group is the least stable. Obviously, the charge distribution on porphyrin depends on the protonation site. The ESP of porphyrin **2** is displayed in Figure 5b. In neutral porphyrin **2**, ESP is negative at the nitrogens on both porphine and pyridyl substituents. When the porphine nitrogen is protonated, the positive charge is delocalized across the porphine plane, resulting in positive ESPs on the plane. On the other hand, when the pyridyl nitrogen is protonated, the positive charge is mostly localized on the protonated pyridyl group, leaving the porphine plane at more negative ESPs than the protonated pyridyl group.

HOMO and LUMO Energies of Porphyrin. To see the effect of protonation on the π – π interaction between porphyrin and fullerene, we calculate the HOMO and LUMO energies of porphyrin. They are listed in Table 2. Orbital energies of fullerene are taken from the experimental data.^{37–39} HOMO energies of C₆₀³⁷ and C₇₀³⁸ are -7.6 and -7.47 eV with a HOMO–LUMO energy gap³⁹ of 1.7 and 1.6 eV, respectively. The HOMO energy of neutral porphyrin ranges from -6.39 to -7.65 eV, with an energy gap of 3.00–3.03 eV. The single protonation on the porphine nitrogen lowers the energy level of HOMO by 3.08–3.62 eV and slightly reduces the energy gap to 2.73–2.79 eV. The double protonation on the porphine nitrogens further stabilizes HOMO by 2.72–3.73 eV with a 2.59–2.71 eV energy gap. Remarkably, the energy levels of HOMO and LUMO of porphyrins vary linearly with the PA of porphine nitrogens, as presented in Figure S1 in the Supporting Information. Meanwhile, the protonation on pyridyl nitrogens in porphyrin **2** successively lowers HOMO by 1.96–2.16 eV, with a nearly identical HOMO–LUMO gap of 2.94–2.97 eV.

Comparison of HOMO and LUMO energies between porphyrin and fullerene suggests that neutral porphyrin donates π -electrons to fullerene because porphyrin HOMO (-6.39 to -7.65 eV) is close to fullerene LUMO (-5.9 eV for both C₆₀ and C₇₀), whereas the protonated porphyrin accepts π -electrons from fullerene because fullerene HOMO (-7.6 to -7.47 eV) is close to LUMO of the protonated porphyrin (-6.72 to -8.18 eV). In porphyrin **2**, fullerene HOMO lies closer to LUMO of **po**¹ than that of **py**¹, but it is closer to LUMO of **py**² than that of **po**¹**py**¹ or **po**².

Binding Energies and Structures of Protonated Porphyrin–Fullerene Complexes. Calculated binding energies of the protonated porphyrin–fullerene complexes are listed in Table 1 for comparison with $E_{50\%}$ values. In the cases of porphyrin–C₇₀ complexes, the binding energies are obtained for both the “end-on” and “side-on” complexes. For singly protonated porphyrins,

the fullerene binding energy is in the range of 14.8–18.5 kcal mol⁻¹, which is approximately one-half the $E_{50\%}$ value of 28–36 kcal mol⁻¹. The C₆₀ binding energy varies from 14.8 to 17.2 kcal mol⁻¹, and the C₇₀ (end-on) binding energy ranges from 15.5 to 17.7 kcal mol⁻¹, which is 0.3–0.8 kcal mol⁻¹ higher than the C₆₀ binding energy.

The C₇₀ (side-on) binding energy is in the range of 15.0–18.5 kcal mol⁻¹, which is 0.6–1.9 kcal mol⁻¹ higher than the C₇₀ (end-on) binding energy for porphyrins **1**–**3** and **5**, but 2.7 kcal mol⁻¹ lower than that for porphyrin **4**. For the doubly protonated porphyrin **2** (**py**²), the C₆₀ binding energy is 22.7 kcal mol⁻¹, and the C₇₀ binding energy is 25.6 (end-on) and 27.6 (side-on) kcal mol⁻¹, which are less than one-half the $E_{50\%}$ values of 56 (loss of C₆₀) and 64 (loss of C₇₀) kcal mol⁻¹. In comparison, the C₆₀ binding energy (19.4 kcal mol⁻¹) for the **po**¹**py**¹ configuration of porphyrin **2** is 3.3 kcal mol⁻¹ less than that for the most stable **py**² conformer; hence, the C₇₀ binding energies for the **po**¹**py**¹ conformer are not calculated.

Structures of singly protonated porphyrin–fullerene complexes are displayed in Figure 6. In all cases, the two protons on the opposite pyrrole nitrogens are pointing toward the electron-rich C=C double bond at the 6:6 ring juncture of fullerene. Of the optimized geometries, the distance between porphyrin and fullerene, the angles between the two opposite pyrrole planes, and the dihedral angles of meso substituents are listed in Table S3 in the Supporting Information. These structural data suggest that the porphyrin–C₇₀ (end-on) binding mode is similar to the porphyrin–C₆₀ binding mode and that the similarity and difference in C₆₀ and C₇₀ binding modes are most apparent in the closest distance between the center of four porphine nitrogens and the 6:6 C=C bond. The porphyrin–fullerene distance for the C₇₀ (end-on) binding (2.73–2.81 Å) is almost identical to that for the C₆₀ binding (2.73–2.82 Å), but 0.16–0.18 Å shorter than that for the C₇₀ (side-on) binding (2.89–2.97 Å). Variation in dihedral angles of meso substituents also indicates that the C₇₀ (side-on) binding exerts more steric repulsion to meso substituents than the C₇₀ (end-on) or C₆₀ binding.

Top and side views of doubly protonated porphyrin **2** (**py**²–fullerene complexes are shown in Figure 7. The porphyrin–fullerene distance in doubly protonated porphyrin **2** (**py**²) decreases by 0.03–0.07 Å from that in singly protonated porphyrin **2** (**po**¹), and yet the porphyrin–C₇₀ (side-on) distance stays 0.16 Å longer than the porphyrin–C₇₀ (end-on) distance. Moreover, the orientation of the 6:6 bond of C₆₀ with respect to the porphine ring is slightly tilted, similarly to the neutral porphyrin–C₆₀ complex.¹⁷ Significantly, the orientation of the

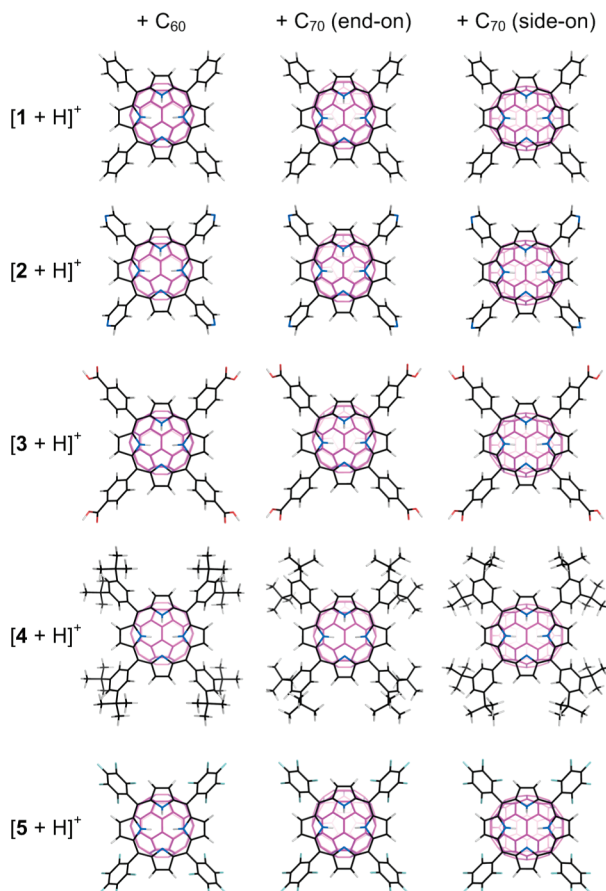


Figure 6. Structures of singly protonated porphyrin–fullerene complexes optimized at the PBE/DZP level.

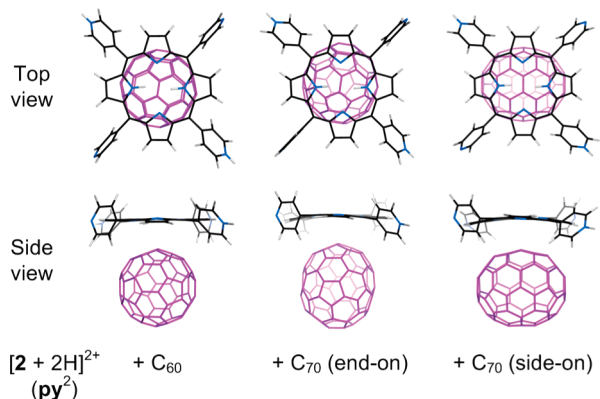


Figure 7. Top and side view of $[2 + 2H]^{2+} \cdot C_{60}$, $[2 + 2H]^{2+} \cdot C_{70}$ (end-on), and $[2 + 2H]^{2+} \cdot C_{70}$ (side-on) complexes in py^2 configuration. The porphyrin plane in $[2 + 2H]^{2+} \cdot C_{60}$ and $[2 + 2H]^{2+} \cdot C_{70}$ (end-on) are planar, and that in $[2 + 2H]^{2+} \cdot C_{70}$ (side-on) is slightly bent. The 6:6 $C=C$ bond of fullerene in $[2 + 2H]^{2+} \cdot C_{60}$ and $[2 + 2H]^{2+} \cdot C_{70}$ (end-on) is slightly tilted from the perpendicular alignment, whereas that in $[2 + 2H]^{2+} \cdot C_{70}$ (side-on) is aligned perpendicular to the plane containing the two protons on the opposite pyrrole nitrogens.

6:6 bond of C_{70} (end-on) is also tilted like C_{60} , but that of C_{70} (side-on) is not.

Discussion

Interaction between Porphyrin and Fullerene. All of the singly protonated porphyrins yield the 1:1 porphyrin–fullerene complexes, whereas only porphyrin **2** of the doubly protonated porphyrins results in the 1:1 complex, suggesting that the twisted saddle structure of the porphyrin doubly protonated on the

porphine center hinders the complex formation. In the case of singly protonated porphyrin, the π -electron system of the slightly puckered porphine plane could interact with the curved π -electron system of fullerene, because the LUMO of protonated porphyrins (-6.72 to -8.18 eV) could accept electrons from the HOMO of fullerene (-7.6 eV for C_{60} and -7.47 eV for C_{70}) lying close in energy.

In the case of doubly protonated porphyrin, however, the HOMO–LUMO interaction between fullerene and porphyrin hardly stabilizes the complex because the porphyrin LUMO (-9.60 to -11.52 eV) lies significantly lower in energy than the fullerene HOMO. Moreover, the saddle structure of porphine disrupts the planar π -electron conjugation, thereby weakening the π – π interaction between porphyrin and fullerene, and the distorted meso substituents sterically hinder the binding of fullerene on the porphine plane. For doubly protonated porphyrin **2**, the 1:1 porphyrin–fullerene complex could be formed from either the po^1py^1 or the py^2 configuration. The most stable configuration py^2 presents a flat porphine plane (Figure 3) for a better contact with fullerene and offers a LUMO (-8.35 eV) close in energy to the fullerene HOMO. The less stable configuration po^1py^1 displays a slightly puckered porphine plane, similarly to the singly protonated porphyrin (po^1) and provides a LUMO (-9.70 eV) located significantly below the fullerene HOMO.

Calculated binding energies of the protonated porphyrin–fullerene complexes are fortuitously close to those of neutral porphyrin–fullerene complexes: The neutral porphyrin–fullerene binding energy and distance calculated at the same DFT/DZP level are 17.3 kcal mol $^{-1}$ and 2.74 Å for the **1**– C_{60} complex, respectively, and 18.4 kcal mol $^{-1}$ and 2.91 Å for the **1**– C_{70} (side-on) complex, respectively. Although the puckered porphine plane in the protonated porphyrin weakens the π – π interaction, the net positive charge localized on the porphine plane seems to attract electron-rich, highly polarizable fullerene.

Meanwhile, the porphyrin–fullerene distance calculated from theory is in good agreement with that reported from crystallographic studies. For instance, crystallographic data show porphyrin–fullerene distances of 2.69 , 2.70 , and ~ 2.74 Å for the neutral **4**– C_{60} , **1**– C_{60} ,¹⁰ and **5**– C_{60} ⁴⁰ complexes, respectively, whereas the present DFT calculation predicts distances of 2.77 , 2.79 , and 2.82 Å for the singly protonated **4**– C_{60} , **1**– C_{60} , and **5**– C_{60} complexes, respectively. This result suggests that, for both neutral and protonated porphyrins, the electron-donating substituents in **4** increase the binding energy and concomitantly shorten the porphyrin–fullerene distance, whereas the electron-withdrawing substituents in **5** decrease the binding energy and extend the distance.

End-On versus Side-On Binding of Fullerene. Previous studies carried out in solution^{4,14} and using high-order theoretical calculations¹⁷ have shown that C_{70} binds more strongly to neutral porphyrin than does C_{60} . The present work shows that C_{70} also binds more strongly to protonated porphyrin than does C_{60} . Moreover, there are two binding modes for C_{70} : one is energetically almost identical to the C_{60} binding, and the other is more stable than the C_{60} binding. The end-on binding mode offers the end cap of C_{70} to the protonated porphyrin, whereas the side-on binding mode offers a side wall with a large contact area to porphyrin. Evidence for the end-on binding of C_{70} is the $E_{50\%}$ values for the loss of C_{70} and C_{60} that are almost identical to each other for both $[4 + H]^+$ and $[5 + H]^+$. Indeed, the calculated binding energies show that the end-on binding of C_{70} is energetically favored over the side-on binding of C_{70} for both protonated porphyrins **4** and **5**, because the C_{70} (side-

on) binding exerts steric repulsion to the meso substituents having either a di-*tert*-butyl group or fluorine. Evidence for the side-on binding of C₇₀ is the *E*_{50%} values for the loss of C₇₀ that are 3–6 kcal mol^{−1} greater than those for the loss of C₆₀ for both protonated porphyrins **1** and **2** having no bulky meso substituents. The calculated binding energy also supports the side-on binding of C₇₀ for protonated porphyrins **1** and **2**.

Effects of Protonation on HOMO–LUMO Energy Gap and on Aggregation. The HF/CIS calculations predict that the HOMO–LUMO energy gap of porphyrin decreases from 3.00–3.03 eV to 2.73–2.79 eV ($\Delta E = -0.23$ to -0.30 eV) upon single protonation on the porphine center and to 2.59–2.71 eV ($\Delta E = -0.31$ to -0.41 eV) upon double protonation. In solution, UV/vis absorption studies have previously shown a decrease in Soret (B)-band energy of porphyrin by protonation under acidic conditions:⁴¹ from 2.99 to 2.86 eV ($\Delta E = -0.13$ eV) for **1**, from 3.00 to 2.82 eV ($\Delta E = -0.18$ eV) for **2**, from 2.95 to 2.81 eV ($\Delta E = -0.14$ eV) for tetra(4-N-methylpyridinium) porphyrin, from 3.01 to 2.64 eV ($\Delta E = -0.37$ eV) for **3**, and from 2.95 to 2.53 eV ($\Delta E = -0.42$ eV) for tetra(4-sulfonatophenyl) porphyrin. These red spectral shifts in protonated porphyrins have also been observed from various tetraphenylporphyrin derivatives in dichloromethane containing sulfuric acid.⁴² Most recent spectroscopic studies in benzonitrile solution have suggested that the B-band of dodecaphenylporphyrin shifts from 2.64 to 2.53 eV ($\Delta E = -0.11$ eV) upon single protonation on the porphine center and to 2.47 eV ($\Delta E = -0.17$ eV) upon double protonation.³¹ This stepwise decrease in B-band transition energy upon successive protonation is in line with the present results.

In addition, it has been reported that protonated porphyrins under acidic conditions readily form *J*-aggregates in slipped facial arrangement of the porphyrins, whereas neutral porphyrins do not.^{41,42} The protonation on the porphine center has been suggested as the primary step toward the formation of aggregates.⁴¹ Our results on the structures, HOMO–LUMO energy gaps, and ESP plots of porphyrins show that the protonation on porphine center induces the rotation of meso-phenyl or -pyridyl group from the perpendicular alignment in neutral porphyrin (Figure 3), reduces the HOMO–LUMO energy gap (Table 2), and delocalizes the positive charge on the porphine plane (Figure 5). Thus, the aromatic meso substituent could be aligned for slipped face-to-face stacking with the protonated porphine plane through π – π and charge-induced dipole interactions, which could lead to the formation of aggregates in the presence of the counteranion in solution.

Conclusion

Combination of energy-dependent CID experiments and the first-principles calculations elucidates the binding mode of fullerene on protonated porphyrins at the molecular level in the absence of solvent and counterions. Porphyrins are readily protonated because of the high proton affinity of the porphine center. Protonated porphyrins form noncovalent complexes with fullerenes through the π – π and charge-induced dipole interactions. The initial complex formation involves the π – π contact interaction rather than the through-space charge-induced dipole interaction. The binding energy of the complex increases as the electron-donating power of meso substituents increases. Porphyrins carrying no bulky substituents on the meso-phenyl or -pyridyl group allow the side-on binding of ovoid C₇₀ on the porphine plane, whereas those having bulky substituents hinder the side-on binding, permitting only the end-on entry of C₇₀.

Acknowledgment. We are grateful to PDW Boyd at the University of Auckland for kindly providing one porphyrin compound. We are thankful for the support from the Functional Proteomics Center (Grant FPR08A1-040) and the National Research Foundation of Korea grant funded by the Korean government (MEST) (Grant 2009-0086218).

Supporting Information Available: Energy levels of HOMO and LUMO of porphyrins as a function of PA, total and zero-point energies of neutral and protonated porphyrins, the changes of energy, zero-point energy and enthalpy, the porphyrin–fullerene distance, dihedral angles of meso substituents, and angles between the pyrrole planes. This material is available free of charge via the Internet at <http://pubs.acs.org>.

References and Notes

- (1) Boyd, P. D. W.; Reed, C. A. Fullerene–Porphyrin Constructs. *Acc. Chem. Res.* **2005**, *38*, 235–242.
- (2) Evans, D. R.; Fackler, N. L. P.; Xie, Z.; Rickard, C. E. F.; Boyd, P. D. W.; Reed, C. A. π -Arene/Cation Structure and Bonding. Solvation versus Ligand Binding in Iron(III) Tetraphenylporphyrin Complexes of Benzene, Toluene, *p*-Xylene, and [60]Fullerene. *J. Am. Chem. Soc.* **1999**, *121*, 8466–8474.
- (3) Hasobe, T.; Imahori, H.; Fukuzumi, S.; Kamat, P. V. Light Energy Conversion Using Mixed Molecular Nanoclusters: Porphyrin and C₆₀ Cluster Films for Efficient Photocurrent Generation. *J. Phys. Chem. B* **2003**, *107*, 12105–12112.
- (4) Hosseini, A.; Taylor, S.; Accorsi, G.; Armaroli, N.; Reed, C. A.; Boyd, P. D. W. Calix[4]arene-Linked Bisporphyrin Hosts for Fullerenes: Binding Strength, Solvation Effects, and Porphyrin–Fullerene Charge Transfer Bands. *J. Am. Chem. Soc.* **2006**, *128*, 15903–15913.
- (5) Kira, A.; Umeyama, T.; Matano, Y.; Yoshida, K.; Isoda, S.; Park, J. K.; Kim, D.; Imahori, H. Supramolecular Donor–Acceptor Heterojunctions by Vectorial Stepwise Assembly of Porphyrins and Coordination-Bonded Fullerene Arrays for Photocurrent Generation. *J. Am. Chem. Soc.* **2009**, *131*, 3198–3200.
- (6) Nojiri, T.; Watanabe, A.; Ito, O. Photoinduced Electron Transfer between C₆₀/C₇₀ and Zinc Tetraphenylporphyrin in Polar Solvents. *J. Phys. Chem. A* **1998**, *102*, 5215–5219.
- (7) D’Souza, F.; Gadde, S.; Zandler, M. E.; Arkady, K.; El-Khouly, M. E.; Fujitsuka, M.; Ito, O. Studies on Covalently Linked Porphyrin–C₆₀ Dyads: Stabilization of Charge-Separated States by Axial Coordination. *J. Phys. Chem. A* **2002**, *106*, 12393–12404.
- (8) Toivonen, T. L. J.; Hukka, T. I.; Cramariuc, O.; Rantala, T. T.; Lemmettyinen, H. DFT and TDDFT Study Related to Electron Transfer in Nonbonded Porphine•C₆₀ Complexes. *J. Phys. Chem. A* **2006**, *110*, 12213–12221.
- (9) Olmstead, M. M.; Costa, D. A.; Maitra, K.; Noll, B. C.; Phillips, S. L.; Van Calcar, P. M.; Balch, A. L. Interaction of Curved and Flat Molecular Surfaces. The Structures of Crystalline Compounds Composed of Fullerene (C₆₀, C₆₀O, C₇₀, and C₁₂₀O) and Metal Octaethylporphyrin Units. *J. Am. Chem. Soc.* **1999**, *121*, 7090–7097.
- (10) Boyd, P. D. W.; Hodgson, M. C.; Rickard, C. E. F.; Oliver, A. G.; Chaker, L.; Brothers, P. J.; Bolskar, R. D.; Tham, F. S.; Reed, C. A. Selective Supramolecular Porphyrin/Fullerene Interactions. *J. Am. Chem. Soc.* **1999**, *121*, 10487–10495.
- (11) Sun, D.; Tham, F. S.; Reed, C. A.; Boyd, P. D. W. Extending Supramolecular Fullerene–Porphyrin Chemistry to Pillared Metal–Organic Frameworks. *Proc. Natl. Acad. Sci.* **2002**, *99*, 5088–5092.
- (12) Yamaguchi, T.; Ishii, N.; Tashiro, K.; Aida, T. Supramolecular Peapods Composed of a Metalloporphyrin Nanotube and Fullerenes. *J. Am. Chem. Soc.* **2003**, *125*, 13934–13935.
- (13) Hasobe, T.; Imahori, H.; Kamat, P. V.; Ahn, T. K.; Kim, S. K.; Kim, D.; Fujimoto, A.; Hirakawa, T.; Fukuzumi, S. Photovoltaic Cells Using Composite Nanoclusters of Porphyrins and Fullerenes with Gold Nanoparticles. *J. Am. Chem. Soc.* **2005**, *127*, 1216–1228.
- (14) Zheng, J.-Y.; Tashiro, K.; Hirabayashi, Y.; Kinbara, K.; Saigo, K.; Aida, T.; Sakamoto, S.; Yamaguchi, K. Cyclic Dimers of Metalloporphyrins as Tunable Hosts for Fullerenes: A Remarkable Effect of Rhodium(III). *Angew. Chem., Int. Ed.* **2001**, *40*, 1858–1861.
- (15) Sun, D.; Tham, F. S.; Reed, C. A.; Chaker, L.; Boyd, P. D. W. Supramolecular Fullerene–Porphyrin Chemistry. Fullerene Complexation by Metalated “Jaws Porphyrin” Hosts. *J. Am. Chem. Soc.* **2002**, *124*, 6604–6612.
- (16) Bonifazi, D.; Spillmann, H.; Kiebele, A.; de Wild, M.; Seiler, P.; Cheng, F.; Güntherodt, H.-J.; Jung, T.; Diederich, F. Supramolecular Patterned Surfaces Driven by Cooperative Assembly of C₆₀ and Porphyrins on Metal Substrates. *Angew. Chem., Int. Ed.* **2004**, *43*, 4759–4763.

- (17) Wang, Y.-B.; Lin, Z. Supramolecular Interactions between Fullerenes and Porphyrins. *J. Am. Chem. Soc.* **2003**, *125*, 6072–6073.
- (18) Jung, Y.; Head-Gordon, M. A Fast Correlated Electronic Structure Method for Computing Interaction Energies of Large van der Waals Complexes Applied to the Fullerene–Porphyrin Dimer. *Phys. Chem. Chem. Phys.* **2006**, *8*, 2831–2840.
- (19) Tashiro, K.; Aida, T.; Zheng, J.-Y.; Kinbara, K.; Saigo, K.; Sakamoto, S.; Yamaguchi, K. A Cyclic Dimer of Metalloporphyrin Forms a Highly Stable Inclusion Complex with C₆₀. *J. Am. Chem. Soc.* **1999**, *121*, 9477–9478.
- (20) Ouchi, A.; Tashiro, K.; Yamaguchi, K.; Tsuchiya, T.; Akasaka, T.; Aida, T. A Self-Regulatory Host in an Oscillatory Guest Motion: Complexation of Fullerenes with a Short-Spaced Cyclic Dimer of an Organorhodium Porphyrin. *Angew. Chem., Int. Ed.* **2006**, *45*, 3542–3546.
- (21) Fenn, J. B.; Mann, M.; Meng, C. K.; Wong, S. F.; Whitehouse, C. M. Electrospray Ionization—Principles and Practice. *Mass Spectrom. Rev.* **1990**, *9*, 37–70.
- (22) Dongré, A. R.; Jones, J. L.; Somogyi, Á.; Wysocki, V. H. Influence of Peptide Composition, Gas-Phase Basicity, and Chemical Modification on Fragmentation Efficiency: Evidence for the Mobile Proton Model. *J. Am. Chem. Soc.* **1996**, *118*, 8365–8374.
- (23) Rodgers, M. T.; Armentrout, P. B. Noncovalent Metal–Ligand Bond Energies as Studied by Threshold Collision-Induced Dissociation. *Mass Spectrom. Rev.* **2000**, *19*, 215–247.
- (24) Ervin, K. M. Experimental Techniques in Gas-Phase Ion Thermochemistry. *Chem. Rev.* **2001**, *101*, 391–444.
- (25) Min, W. J.; Jung, S.; Lim, S. J.; Kim, Y.; Shin, S. K. Collision-Induced Dissociation of II-VI Semiconductor Nanocrystal Precursors, Cd²⁺ and Zn²⁺ Complexes with Trioctylphosphine Oxide, Sulfide, and Selenide. *J. Phys. Chem. A* **2009**, *113*, 9588–9594.
- (26) Frisch, M. J.; Trucks, G. W.; Schlegel, H. B.; Scuseria, G. E.; Robb, M. A.; Cheeseman, J. R.; Montgomery, J. A., Jr.; Vreven, T.; Kudin, K. N.; Burant, J. C.; Millam, J. M.; Iyengar, S. S.; Tomasi, J.; Barone, V.; Mennucci, B.; Cossi, M.; Scalmani, G.; Rega, N.; Petersson, G. A.; Nakatsuji, H.; Hada, M.; Ehara, M.; Toyota, K.; Fukuda, R.; Hasegawa, J.; Ishida, M.; Nakajima, T.; Honda, Y.; Kitao, O.; Nakai, H.; Klene, M.; Li, X.; Knox, J. E.; Hratchian, H. P.; Cross, J. B.; Adamo, C.; Jaramillo, J.; Gomperts, R.; Stratmann, R. E.; Yazyev, O.; Austin, A. J.; Cammi, R.; Pomelli, C.; Ochterski, J. W.; Ayala, P. Y.; Morokuma, K.; Voth, G. A.; Salvador, P.; Dannenberg, J. J.; Zakrzewski, V. G.; Dapprich, S.; Daniels, A. D.; Strain, M. C.; Farkas, O.; Malick, D. K.; Rabuck, A. D.; Raghavachari, K.; Foresman, J. B.; Ortiz, J. V.; Cui, Q.; Baboul, A. G.; Clifford, S.; Cioslowski, J.; Stefanov, B. B.; Liu, G.; Liashenko, A.; Piskorz, P.; Komaromi, I.; Martin, R. L.; Fox, D. J.; Keith, T.; Al-Laham, M. A.; Peng, C. Y.; Nanayakkara, A.; Challacombe, M.; Gill, P. M. W.; Johnson, B.; Chen, W.; Wong, M. W.; Gonzalez, C.; Pople, J. A. *Gaussian 03*, Revision B.04; Gaussian, Inc.: Pittsburgh, PA, 2003.
- (27) Scott, A. P.; Radom, L. Harmonic Vibrational Frequencies: An Evaluation of Hartree–Fock, Møller–Plesset, Quadratic Configuration Interaction, Density Functional Theory, and Semiempirical Scale Factors. *J. Phys. Chem.* **1996**, *100*, 16502–16513.
- (28) Lias, S. G.; Liebman, J. F.; Levin, R. D. Evaluated Gas Phase Basicities and Proton Affinities of Molecules; Heats of Formation of Protonated Molecules. *J. Phys. Chem. Ref. Data* **1984**, *13*, 695–808.
- (29) Fonseca Guerra, C.; Snijder, J. G.; te Velde, G.; Baerends, E. J. Towards an Order-N DFT Method. *Theor. Chem. Acc.* **1998**, *99*, 391–403.
- (30) te Velde, G.; Bickelhaupt, F. M.; van Gisbergen, S. J. A.; Fonseca Guerra, C.; Baerends, E. J.; Snijders, J. G.; Ziegler, T. Chemistry with ADF. *J. Comput. Chem.* **2001**, *22*, 931–967.
- (31) Honda, T.; Kojima, T.; Fukuzumi, S. Crystal Structures and Properties of a Monoprotonated Porphyrin. *Chem. Commun.* **2009**, 4994–4996.
- (32) Vinokur, N.; Ryzhov, V. Using Collision-Induced Dissociation with Corrections for the Ion Number of Degrees of Freedom for Quick Comparison of Relative Bonding Strength. *J. Mass Spectrom.* **2004**, *39*, 1268–1274.
- (33) Laskin, J.; Bailey, T. H.; Futrell, J. H. Fragmentation Energetics for Angiotensin II and Its Analogs from Time- and Energy-Resolved Surface-Induced Dissociation Studies. *Int. J. Mass Spectrom.* **2004**, *234*, 89–99.
- (34) Chen, D.-M.; Liu, X.; He, T.-J.; Liu, F.-C. Density Functional Theory Investigation of Porphyrin Diacid: Electronic Absorption Spectrum and Conformational Inversion. *Chem. Phys.* **2003**, *289*, 397–407.
- (35) McElvany, S. W.; Callahan, J. H. Chemical Ionization of Fullerenes. *J. Phys. Chem.* **1991**, *95*, 6186–6191.
- (36) Wheeler, S. E.; Houk, K. N. Through-Space Effects of Substituents Dominate Molecular Electrostatic Potentials of Substituted Arenes. *J. Chem. Theory Comput.* **2009**, *5*, 2301–2312.
- (37) Lichtenberger, D. L.; Nebesny, K. W.; Ray, C. D.; Huffman, D. R.; Lamb, L. D. Valence and Core Photoelectron Spectroscopy of C₆₀, Buckminsterfullerene. *Chem. Phys. Lett.* **1991**, *176*, 203–208.
- (38) Lichtenberger, D. L.; Rempe, M. E.; Gogosha, S. B. The He I Valence Photoelectron Spectrum of C₇₀ in the Gas Phase. *Chem. Phys. Lett.* **1992**, *198*, 454–460.
- (39) Haufler, R. E.; Wang, L.-S.; Chibante, L. P. F.; Jin, C.; Conceicao, J.; Chai, Y.; Smalley, R. E. Fullerene Triplet State Production and Decay: R2PI Probes of C₆₀ and C₇₀ in a Supersonic Beam. *Chem. Phys. Lett.* **1991**, *179*, 449–454.
- (40) Hosseini, A.; Hodgson, M. C.; Tham, F. S.; Reed, C. A.; Boyd, P. D. W. Tapes, Sheets, and Prisms. Identification of the Weak C–F Interactions that Steer Fullerene–Porphyrin Cocrystallization. *Cryst. Growth Des.* **2006**, *6*, 397–403.
- (41) Akins, D. L.; Zhu, H.-R.; Guo, C. Aggregation of Tetraaryl-Substituted Porphyrins in Homogeneous Solution. *J. Phys. Chem.* **1996**, *100*, 5420–5425.
- (42) Okada, S.; Segawa, H. Substituent-Control Exciton in J-Aggregates of Protonated Water-Insoluble Porphyrins. *J. Am. Chem. Soc.* **2003**, *125*, 2792–2796.

JP1033855